Bounds on strain in large Tertiary shear zones of SE Asia from boudinage restoration

R. LACASSIN, P.H. LELOUP and P. TAPPONNIER

Laboratoire de Tectonique, Mécanique de la Lithosphère, U.R.A. 1093 CNRS, Institut de Physique du Globe de Paris, 4 place Jussieu, 75252 Paris Cédex 05, France

Abstract—We have used surface-balanced restoration of stretched, boudinaged layers to estimate minimum amounts of finite strain in the mylonitic gneisses of the Oligo-Miocene Red River–Ailao Shan shear zone (Yunnan, China) and of the Wang Chao shear zone (Thailand). The layer-parallel extension values thus obtained range between 250 and 870%. We discuss how to use such extension values to place bounds on amounts of finite shear strain in these large crustal shear zones. Assuming simple shear, these values imply minimum total and late shear strains of, respectively, 33 ± 6 and 7 ± 3 at several sites along the Red River–Ailao Shan shear zone. For the Wang Chao shear zone a minimum shear strain of 7 ± 4 is deduced. Assuming homogeneous shear would imply that minimum strike-slip displacements along these two left-lateral shear zones, which have been interpreted to result from the India–Asia collision, have been of the order of 330 ± 60 km (Red River–Ailao Shan) and 35 ± 20 km (Wang Chao).

INTRODUCTION

PLATE-scale kinematic reconstructions of past continental deformations require not only the recognition and dating of large brittle or ductile shear zones, but also quantitative assessment of the direction, sense and amount of movement. The geometry of foliations and stretching lineations (e.g. Escher & Watterson 1974, Mattauer 1975, Berthé *et al.* 1979, Mattauer *et al.* 1981, Malavieille *et al.* 1984), and the use of shear criteria (e.g. Simpson & Schmid 1983), now commonly permits determination of the direction and sense of movement in most crustal-scale shear zones. Intense strain in rocks is often qualitatively indicated by the presence of pervasive mylonitic textures (Bell & Etheridge 1973, White *et al.* 1980), sheath folds or 'a'-folds (Quinquis *et al.* 1978, Cobbold & Quinquis 1980, Malavieille 1987), large-scale foliation boudinage (Gaudemer & Tapponnier 1987, Lacassin 1988) or rolling structures (Passchier & Simpson 1986, Van Den Driessche 1986, Van Den Driessche & Brun 1987). The occurrence of well-developed sheath folds (Lacassin & Mattauer 1985) or of foliation boudinage (Gaudemer & Tapponnier 1987) for instance, has been used to infer shear strains (γ) of at least 20, assuming that their formation was due to simple shearing.

To date, however, few attempts have been made at measuring values or bounds of finite strains in large-scale shear zones. Such zones are generally affected by strong recrystallization due to syntectonic metamorphism which has obliterated most or all pretectonic markers such as fossils or pebbles. Techniques of strain measurement that are efficient in less deformed sedimentary rocks are thus inadequate (e.g. Ramsay & Huber 1983). In metamorphic or granitoid rocks, the finite strain may be obtained from xenolith shapes (Ramsay & Allison 1979), from the geometric distribution of porphyroclasts (Fry 1979, Lacassin & Van Den Driessche 1983, Saltzer & Hodges 1988) or from folded or boudinaged veins (Talbot 1970). In large shear zones however, the highly strained state of rocks generally precludes the use of these techniques. Useful applications of Fry's technique, for example, seem to be restricted to strain ratios $X/Z \leq 12$ (Lacassin & Van Den Driessche 1983) and to the case in which the objects present at the beginning of the deformation are still recognizable. It does not hold in mylonites where clast development is important. Talbot's method requires sets of veins with varied orientations to define extension and shortening sectors, a condition difficult to find in mylonites where markers have usually been transposed by the intense strain. In certain cases, generally for small-scale shear zones, it has been possible to estimate the shear strains from the deflection of the foliation or of markers across the shear zone (e.g. Coward 1976, Burg & Laurent 1978, Ramsay & Allison 1979). This is generally not feasible in crustal shear zones with large offsets, mostly because the continuity of foliations or geological markers across such zones is lost.

In this work we use a new method to restore the large extension of boudinaged layers or veins. Examples are taken from two crustal shear zones in SE Asia (Fig. 1) that have been interpreted to result from the India–Asia collision: the Red River–Ailao Shan shear zone, Yunnan, China (Tapponnier *et al.* 1986, 1990, Peltzer & Tapponnier 1988, Zhong Dalai *et al.* 1990, Leloup 1991, Leloup *et al.* submitted), and the Wang Chao shear zone, NW Thailand (Tapponnier *et al.* 1986, Lacassin *et al.* 1991). Estimates of the total displacements on these fault zones have been derived from the offset of geological markers (Tapponnier *et al.* 1986, 1990, Leloup 1991, Leloup *et al.* submitted), from the reconstruction of the South China Sea that probably opened as a pull apart at the termination of the Red River–Ailao Shan fault zone
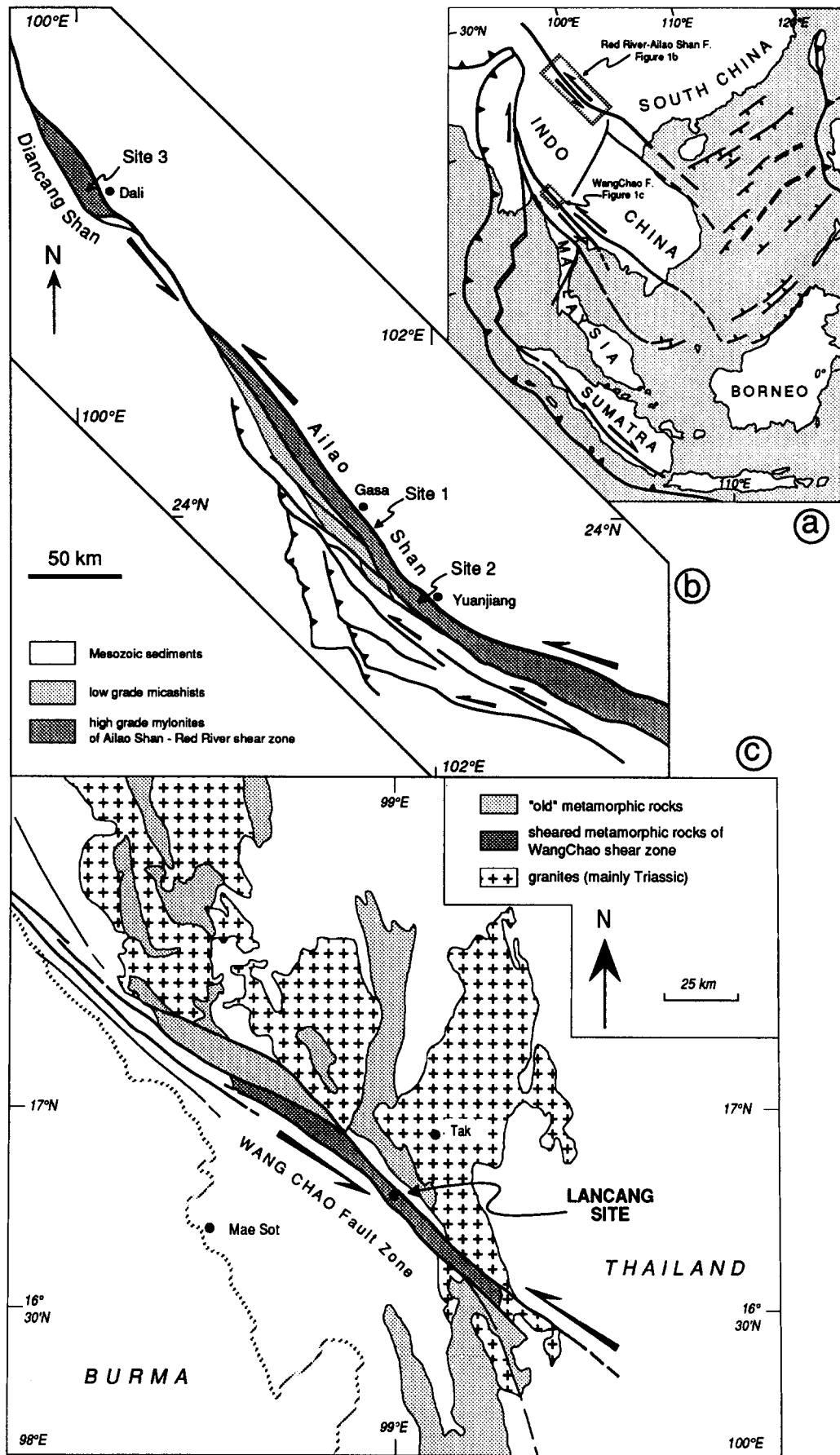
Fig. 1. (a) Map of major Tertiary faults of SE Asia (after Peltzer & Tapponnier 1988) showing location of finite strain studies. (b) Schematic structural sketch map of the Red River–Ailao Shan shear zone (after Tapponnier *et al.* 1990 and Leloup *et al.* submitted). Sites 1, 2 and 3 refer to locations where boudin trails were mapped for quantitative study (see Table 1). (c) Schematic structural sketch map of the Wang Chao shear zone (Department of Mineral Resources 1982, Lacassin *et al.* in preparation) showing location of finite strain measurement site.

(Briais 1989, Briais et al. in press), or from models that predict extrusion-related displacements (Tapponnier et al. 1986, Peltzer & Tapponnier 1988). It follows that left-lateral movements ranging between 500 and 740 km might have occurred on the Red River–Ailao Shan fault zone during the Tertiary. A left-lateral movement of 160–200 km may also be estimated for the Wang Chao fault zone. Despite the uncertainties on these estimates, there is little doubt that we deal with crustal or lithospheric-scale faults with offsets of several hundreds of kilometres. In the light of these possible values of total movement, we thus explore and discuss the use of the extension measurements to place first-order bounds of the shear strain in these shear zones, and hence of the displacement achieved by ductile shear.

GEOLOGICAL AND TECTONIC SETTING

The Red River–Ailao Shan and Wang Chao fault zones are marked by elongated cores of metamorphic rocks a few kilometers wide ($\approx$8–10 km in the Ailao Shan and Diancang Shan and $\approx$5 km in the Wang Chao zone near Lancang National Park). These cores are chiefly made of mylonitic paragneisses and orthogneisses with steep foliations (dips are generally $\geq$70°) and nearly horizontal stretching lineations, in which clear left-lateral shear criteria of various types are ubiquitous (Tapponnier et al. 1990, Lacassin et al. 1991, Leloup 1991, Leloup et al. submitted).

Along the Red River–Ailao Shan zone the mylonites formed under amphibolite facies metamorphic conditions ($P \approx 4.5 \pm 1.5$ kb, $T \approx 710 \pm 70°$C; Leloup 1991, Leloup & Kienast submitted). The northeastern part of the Ailao Shan massif, as well as the eastern part of the Diancang Shan massif, is formed of thinly banded mylonitic paragneisses that include amphibolite layers, migmatitic zones and boudins of marbles and skarns (Leloup & Kienast submitted, Leloup et al. submitted). According to Tapponnier et al. (1990) and Leloup & Kienast (submitted) this rock assemblage probably resulted from the deformation and metamorphism of the sedimentary cover of the Yangtse platform (Devonian and Permian limestones, Permian basalts, Mesozoic sandstones and pelites) that outcrops unmetamorphosed on the north side of the metamorphic core. The left-lateral shearing of these rocks took place at a high temperature (>600°C), corresponding to the metamorphic peak under amphibolite facies, and continued during the retrograde evolution under greenschist facies (Leloup 1991, Leloup & Kienast submitted). Several generations of leucocratic veins, of which the less deformed have been dated at $\approx$23 Ma (U/Pb, Schärer et al. 1990), result from syntectonic partial melting. These veins and the amphibolite layers, which are parallel to the mylonitic banding, are stretched along the shear zone and form spectacular trails of boudins generally parallel to the foliation (Figs. 2 and 3). Localized thinning (pinch and swell structure) and the asymmetric shape of the boudin elements show that the stretched

veins have been penetratively deformed during boudinage. We have measured finite elongation along several trails of boudins from three different sites in the Ailao Shan and Diancang Shan massifs (Figs. 1b, 2b & c and 3, and Table 1).

In contrast with the Ailao Shan and Diancang Shan, where high-grade metamorphism was clearly coeval with shear, the mylonitic core of the Wang Chao shear zone seems to be made of reworked metamorphic rocks in the greenschist facies. The N–S-trending zone of gneisses and granitic intrusions that extends across northwestern Thailand bends into the shear zone (Department of Mineral Resources 1982), and typical rock assemblages, visible several tens of kilometres north of the shear zone, are found mylonitized along it. Here we measured the elongation of leucocratic veins that showed boudinage structures similar to those seen along the Red River–Ailao Shan shear zone. We present the results obtained at one site located at the entrance of the Lancang National Park (Site 4, Fig. 1c and Table 2), $\approx$2 km northeast of the central ultramylonitic part of the shear zone. Farther outside the shear zone, veins of the same type are found undeformed (Fig. 2a) and generally parallel to an older N–S foliation.

In both shear zones, deformed rocks have a strong L–S tectonite fabric and display outstanding stretching lineations that are everywhere nearly horizontal. These characteristics suggest nearly plane strain. In the YZ plane (perpendicular to lineation), the mylonitic banding and the veins are generally not stretched and may locally display small-scale folds that appear to be sections of sheath folds or 'a'-folds (Quinquis et al. 1978, Malavieille 1987). The various shear criteria are mutually consistent and imply left-lateral shear sense at all sites we studied (Tapponnier et al. 1990, Leloup 1991, Leloup et al. submitted). The fact that we were unable to find shear criteria opposite to the bulk shear sense suggests that deformation was probably close to simple shear. It has been argued that the presence of asymmetric boudinage and 'extensional' shear planes would be typical of general non-coaxial flows that deviate from simple shear (e.g. Hanmer & Passchier 1991). However, extensional shears inclined to the bulk shear plane and synthetic to the bulk shearing have been produced in many simple shear experiments of both isotropic and anisotropic models (e.g. Riedel 1929, Tchalenko 1970, Harris & Cobbold 1984) and are widespread in shear zones. Furthermore, we did not observe the conjugate shears that are likely to form in general non-coaxial flow (Platt & Vissers 1980). Most of the boudin trails we studied (Figs. 2 and 3) appear to have formed as pinch-and-swell structures with shear planes located in pinches ('Type 2 asymmetric pulled-apart' of Hanmer 1986). This type of structure may form in simple shearing provided that slip may locally occur on the foliation or layer anisotropy, and that boudin elements rotate backward relative to the bulk shear sense (Harris & Cobbold 1984, Hanmer 1986). Thus, the elongation of the whole boudin trail will probably be close to the layer-parallel extensional strain that would result from bulk simple

shear. Hanmer (1990) and Hanmer & Passchier (1991) have also argued that in a true simple shear regime, the wings of rolling structures might have a stair-step geometry relative to the shear plane (wings are flats linked by the rotating core and parallel to the shear plane, and are not aligned in a single plane). We often observed rolling structures with such stair-step geometry, including mature 'delta-type' ones (Passchier & Simpson 1986, Hanmer 1990), mixed with others that looked 'in-plane' (wings lie in a single plane parallel to the shear plane— Hanmer 1990, Hanmer & Passchier 1991) in the same outcrop. Further discussion of the most subtle differences between true simple shear and general non-coaxial flow regimes is beyond the scope of this paper. In view of the evidence summarized above, however, we find it justified to assume that small-scale deformation was probably close to simple shearing in the two shear zones we studied. Moreover, at a larger scale, the inference of nearly plane strain and simple shear is supported by the absence of an important crustal root under the shear zone (Yan Qizhong et al. 1985) and by the fact that, for a shear zone of such length, there is no way to absorb an important component of flattening normal to the shear zone by horizontal lengthening of the shear zone walls. Nor is there any field evidence for such lengthening.

MEASUREMENT OF LAYER-PARALLEL STRETCHING OF AMPHIBOLITE OR LEUCOCRATIC BOUDIN TRAILS

In both strike-slip shear zones, the boudin trails were studied on flat, nearly horizontal, water-polished outcrops. The observation planes were thus nearly perpendicular to the shear plane and contained the stretching lineation or shear direction (XZ plane). Mapping of the outcrops was performed directly in the field or on scaled photographs taken in the field. This yielded drawings of trails of boudins often several metres long. The drawings were then digitized, the different boudin elements being drawn as curvilinear polygons on a Macintosh computer (e.g. Fig. 4a).

To estimate the amount of extension we first restored the gaps between the boudins (Fig. 4b) by connecting their tails. For boudins that were clearly separated by shear-planes, we also restored the corresponding shear displacements (Fig. 4c) but we were unable to take the rotation of the boudin elements into account. Such restoration is the usual way of obtaining stretch measurements from boudinage structures (Ramsay 1967, p. 247). It is thought to be adequate for boudinage of layers with strong rheological contrast (i.e. stiff layers in a ductile matrix). More sophisticated methods could be used to fit the boudins (e.g. Ferguson 1981) but would still underestimate the finite elongation of penetratively deformed layers or veins. Indeed, such veins do not restore to a regular thickness and still present pinch-and-swell structures where the thinned boudin tails join (e.g. Figs. 4, 6 and 7). Most of the undeformed veins, as north

of the Wang Chao shear zone (Fig. 2a), or only slightly deformed veins, as the latest anatectic veins in the Red River–Ailao Shan shear zone (Figs. 3b and 8), have a regular thickness. Therefore, in a third step we restored the boudinaged layers to constant thickness using surface balancing. The surface of each element in the deformed state was measured as well as the thickness of the thickest boudin element, which was assumed to be close to the thickness of the layer before boudinage (Fig. 4). Note that for elongate boudin elements, which may be oblique to the foliation, the thickness was measured perpendicular to the long axis of the boudins (see, for example, Figs. 10 and 11). Assuming that the total surface of the whole boudin trail remained constant during that part of the finite shear history that led to boudinage, it is possible to reconstruct a layer of constant thickness (Fig. 4d). The use of surface balancing implies that plane strain and no volume change conditions are verified. Deviations from these conditions, such as flattening normal to the shear zone accommodated by vertical extension, or volume loss normal to the shear zone walls, would have induced a thinning of the veins. Thus, in any of these cases, as the initial thickness is underestimated, surface balancing yields lower bounds of the layer-parallel elongation in the XZ plane. In general the reconstruction is not unique. When there are many large elements and several ways to measure the thickness of the elements, several restorations are possible (e.g. Figs. 8b and 10 or 11).

The total layer-parallel extension in the plane of observation is given by:

$$e = (l_1 - l_0)/l_0$$

(e.g. Ramsay 1967, Ramsay & Huber 1983),

l_0 and l_1 being the lengths of the restored layer and of the boudin trail, respectively. Note that $e = 1$ means that the extension is 100% and the length of the deformed layer is twice its original length. $\lambda = (1 + e)^2$ is the quadratic extension (e.g. Ramsay 1967, Ramsay & Huber 1983).

The principal uncertainties in the stretching measurements thus obtained result from two main types of errors. The first type is due to sampling of the boudin trails on the outcrops. To avoid problems due to the irregular spacing and the variable size of the boudin elements, one should in principle map trails of great length. In practice, this proves to be quite difficult. Errors resulting from such sampling bias, that lead to under- or overestimates of the true strain, are illustrated in Fig. 5. Another illustration of this type of error is given by the restoration of sample A1 (Fig. 9). The restoration of parts of this boudin trail ($1'$ to $1'''$) gives variable extension values, lower than that which results from the restoration of the whole trail. The discrepancy is due not only to the irregular spacing of the pulled-apart elements but also to the fact that different thicknesses are used to restore the different parts of the trail. Sampling bias may lead either to under- or overestimates, but practical field sampling of boudin trails will in general yield minimum estimates of the true strain. In
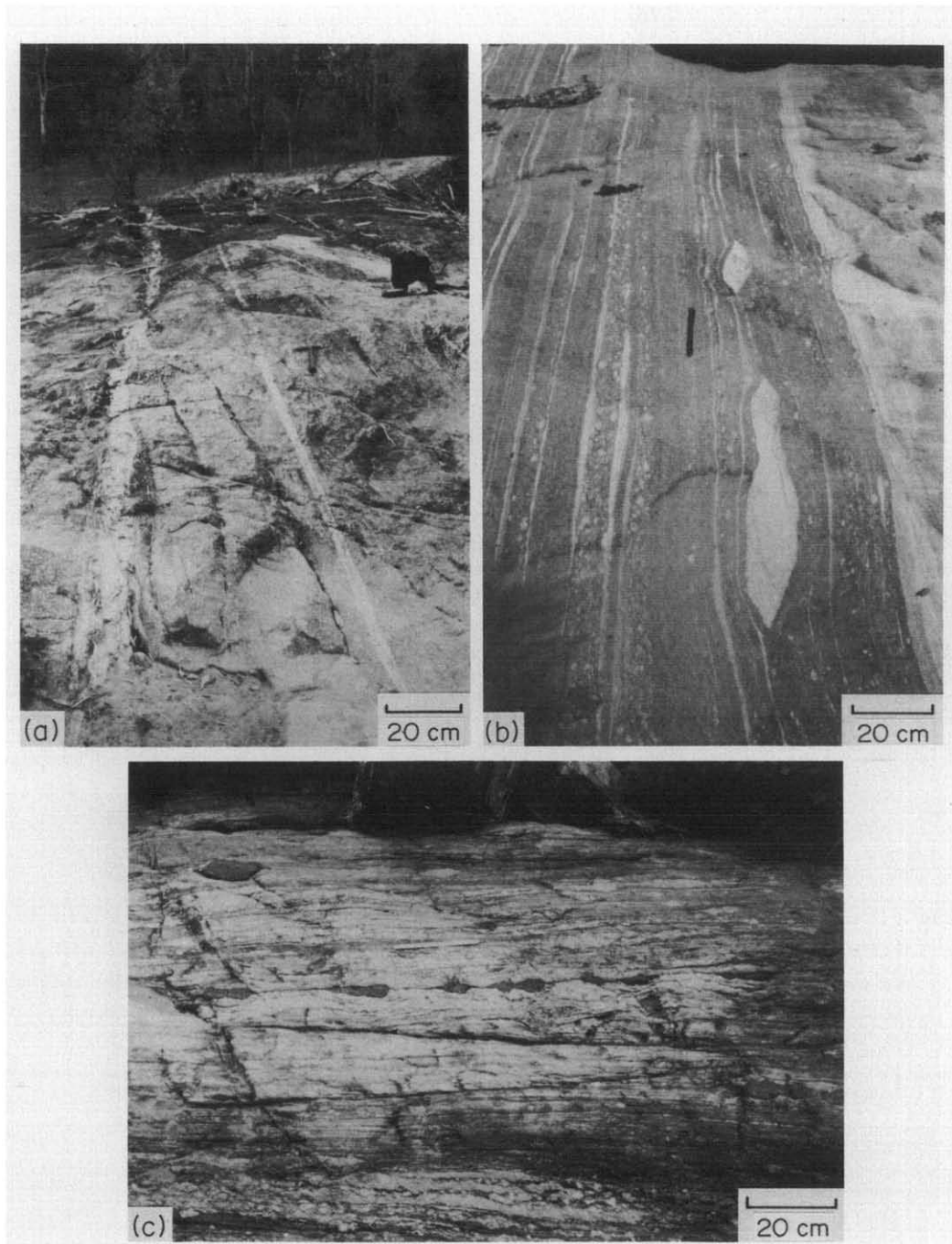
Fig. 2. (a) Initial geometry of leucocratic veins outside the Wang Chao shear zone. Most veins strike N–S and have uniform thicknesses. (b) Example of stretched leucocratic veins at site 2 (Yuan Jiang section, Ailao Shan). Note that boudin elements are asymmetric and separated by large gaps. (c) Example of amphibolite boudins at site 1 (north of Gasa, Ailao Shan).
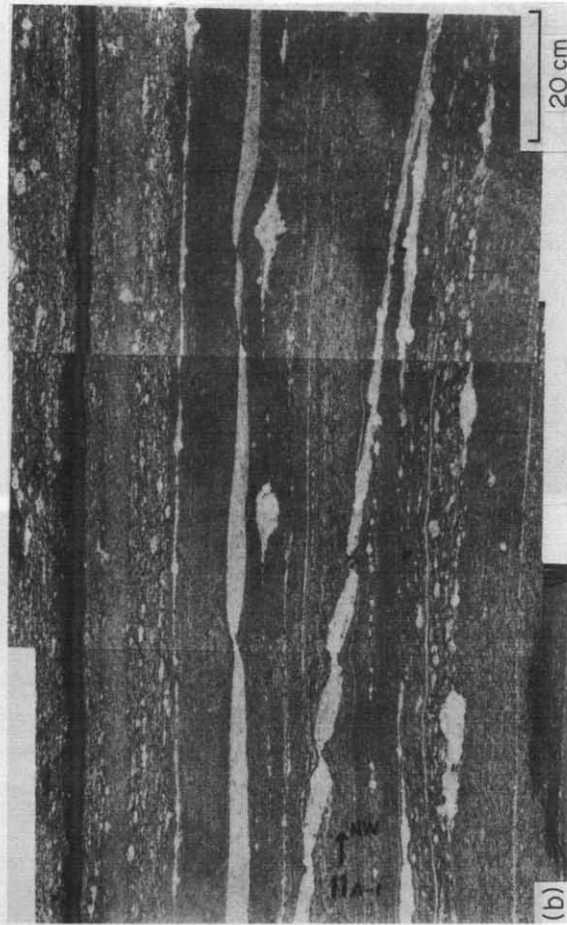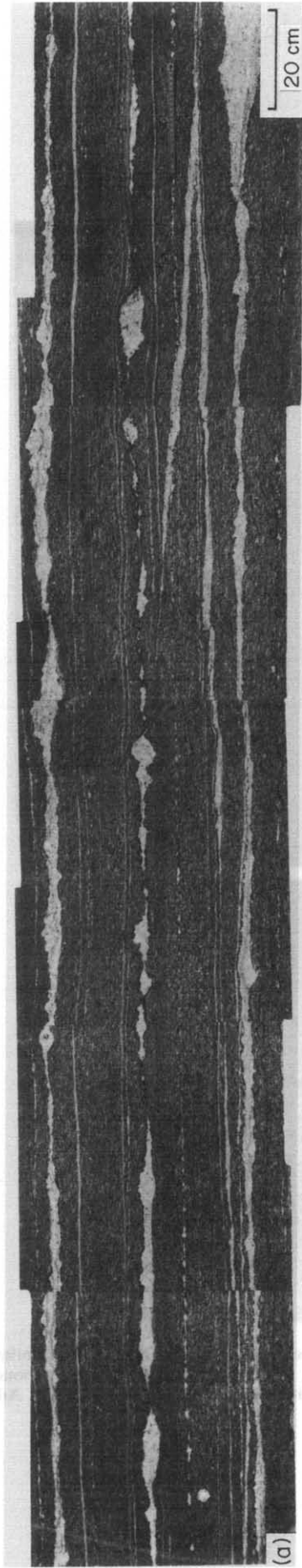
Table 1. Results of constant-area boudinage restoration in the Red River–Ailao Shan shear zone. Italics: less reliable results (see remarks in right column); bold lettering: most reliable results; underlined lettering: alternative results corresponding to alternative initial thicknesses (for certain samples). l_1 and l_0 are length of observed boudin trail and restored layer length, respectively. t is restored layer thickness. e is layer-parallel extension and λ is quadratic extension (see Fig. 4)

Yunnan		l_1 (cm)	l_0 (cm)	t (cm)	e	e (%)	λ			
Boudin A		*181.6*	*59.1*	*10.8*	*2.07*	*207*	*9.4*	Leucocratic vein, site 2 (Yuan Jiang)		Sample length insufficient
Boudin B		**255.7**	**37.1**	**12.2**	**5.89**	**589**	**47.5**	Amphibolite layer, site 1 (SW of Gasa)	Fig. 4	
Boudins C	*(1)*	*111.9*	*34.0*	*10.8*	*2.29*	*229*	*10.8*			
	2	**286.9**	**29.7**	**7.6**	**8.66**	**866**	**93.3**	Amphibolite layers, site 1 (SW of Gasa)	Fig. 6	Length of samples 1 and 6 is insufficient
	3	**302.9**	**33.8**	**8.5**	**7.96**	**796**	**80.3**			
	4	**383.7**	**43.3**	**10.5**	**7.86**	**786**	**78.5**			
	5	**412.8**	**57.6**	**16.9**	**6.17**	**617**	**51.4**			
	(6)	*121.2*	*49.6*	*8.4*	*1.44*	*144*	*6.0*			
Boudins D	**1**	**160.0**	**26.1**	**1.1**	**5.13**	**513**	**37.6**	Leucocratic veins, site 2 (Yuan Jiang)	Fig. 7	
	2	**299.5**	**67.2**	**5.0**	**3.46**	**346**	**20.0**			
Boudins E	**1**	**114.7**	**15.1**	**4.4**	**6.6**	**660**	**57.7**			
		<u>114.7</u>	<u>13.3</u>	<u>5.0</u>	<u>7.62</u>	<u>762</u>	<u>74.4</u>			
		<u>114.7</u>	<u>17.0</u>	<u>3.9</u>	<u>5.75</u>	<u>575</u>	<u>45.5</u>			
	2	**130.3**	**24.2**	**3.8**	**4.38**	**438**	**29.0**	Leucocratic veins, site 2 (Yuan Jiang)	Fig. 8	
		<u>130.3</u>	<u>34.0</u>	<u>2.7</u>	<u>2.83</u>	<u>283</u>	<u>14.7</u>			
	3	**123.9**	**33.7**	**2.7**	**2.68**	**268**	**13.5**			
	(4)	*132.3*	*88.8*	*2.8*	*0.49*	*49*	*2.22*			Samples 4 and 5 are late syntectonic veins
	(5)	*133.9*	*68.7*	*2.9*	*0.95*	*95*	*3.8*			
DCS boudins	**1**	**110.0**	**20.8**	**4.6**	**4.29**	**429**	**28.0**	Leucocratic veins, site 3 (Diancang Shan)		
	2	**79.9**	**10.6**	**3.6**	**6.54**	**654**	**56.9**			

fact, one generally ceases to draw or to photograph the trails when the gaps between the boudins become too large. We believe it is likely that we sampled mostly segments of the trails where the density of boudin elements was high (e.g. a in Fig. 5).

Another type of error derives from uncertainty in the determination of the initial layer thickness (Figs. 8b, 10 and 11 for instance). Note however that, the layers being penetratively deformed, the initial thicknesses of the layers must have been larger than the thickness of the thickest boudin elements used to construct the restored layer.

Therefore, in general, restoration of boudin trails

based on surface balancing should provide minimum estimates of the finite extension of such trails.

RESULTS

The results are presented in Tables 1 and 2 for the Red River–Ailao Shan shear zone and the Wang Chao shear zone, respectively. Numbers in italic in Table 1 refer to less reliable results, generally because the boudin trail was clearly too short (e.g., Fig. 6), and these are not integrated into the following discussion. Samples E4 and E5 obviously correspond to late syntectonic veins (Figs.

Table 2. Results of constant-area boudinage restoration in the Wang Shao–Lancang shear zone. Symbols and lettering as in Table 1

| Thailand		l_1 (cm)	l_0 (cm)	t (cm)	e	e (%)	λ		
Boudin A	<u>1'</u>	<u>129.8</u>	<u>18.5</u>	<u>4.3</u>	<u>6.02</u>	<u>602</u>	<u>49.3</u>		Sample A1 has been divided into three sections (1',
	<u>1"</u>	<u>239.9</u>	<u>29.5</u>	<u>2.5</u>	<u>7.13</u>	<u>713</u>	<u>66.1</u>		1" and 1''')
	<u>1'''</u>	<u>166.9</u>	<u>25.4</u>	<u>3.3</u>	<u>3.71</u>	<u>371</u>	<u>22.2</u>	Fig. 9	
	1	**539.8**	**60.9**	**4.3**	**7.86**	**786**	**78.5**		
	2	**177.1**	**48.5**	**2.1**	**2.65**	**265**	**13.3**		
	3	**108**	**27**	**2.1**	**3.0**	**300**	**16**		
Boudin B	**1**	**411**	**62.4**	**9.4**	**5.59**	**559**	**43.5**		All samples are leucocratic veins from Lancang Site
		<u>411</u>	<u>117.4</u>	<u>5.0</u>	<u>2.5</u>	<u>250</u>	<u>12</u>	Fig. 10	(site 4)
	2	**403.4**	**76.3**	**3.4**	**4.28**	**428**	**28**		
		<u>403.4</u>	<u>99.8</u>	<u>2.6</u>	<u>3.04</u>	<u>304</u>	<u>16</u>		
Boudin C	**1**	**533.7**	**119.7**	**18.2**	**3.45**	**345**	**20**		
		<u>533.7</u>	<u>165</u>	<u>13.2</u>	<u>2.23</u>	<u>223</u>	<u>10.5</u>		
	2	**359.3**	**74.7**	**1.8**	**3.81**	**381**	**23**	Fig. 11	
		<u>359.3</u>	<u>89.7</u>	<u>1.5</u>	<u>3.01</u>	<u>301</u>	<u>16</u>		
Boudin D		**212.1**	**53.6**	**1.2**	**2.96**	**296**	**16**		
		<u>212.1</u>	<u>64.4</u>	<u>1.0</u>	<u>2.29</u>	<u>229</u>	<u>11.5</u>		
Boudin E		**258.8**	**40.8**	**5.7**	**5.34**	**534**	**40.2**		
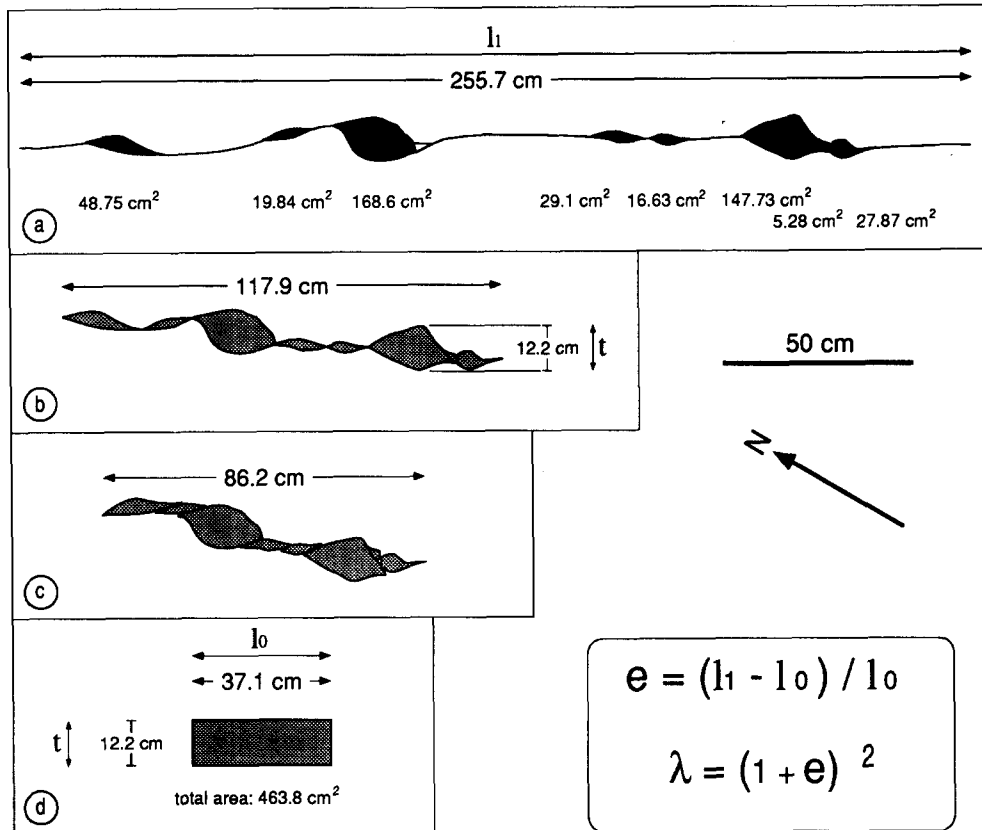
Fig. 4. Mapped amphibolite boudins (sample B, site 1, Ailao Shan) showing method used for boudinage restoration. (a) Digitized boudin trail (derived from field mapping); (b) fit of boudin tips; (c) restoration of movement on shear planes; (d) final restoration by surface balancing. Initial thickness of restored layer is taken to be the thickness (t) of the thickest boudin element. Thickness is measured perpendicular to the long axis of elongate elements. l_1 is observed length of boudin trail; l_0 is the restored initial layer length.

3b and 8) and the extension values obtained for these samples (also in italic on Table 1) reflect only the latest strain increments.

Red River–Ailao Shan shear zone

At site 1, southwest of Gasa at the northeastern edge of the Ailao Shan metamorphic core (Figs. 1b, 4 and 6), the reliable results obtained for layer-parallel extension of amphibolite layers range between 589 and 866% (samples B and C, Table 1). From these results, a mean

extension of 733% may be deduced for this site (the mean quadratic extension being 70.5).

At site 2, near the axis of the Ailao Shan metamorphic core on the Yuan Jiang section (Figs. 1b, 7 and 8) (fig. 2 in Tapponnier *et al.* 1990), the reliable values of extension range between 268 and 660% (samples A, D and E, Table 1), yielding a mean extension of 505% (a mean quadratic extension 31.6).

Site 3 is located within the Diancang Shan massif, west of Dali (Fig. 1b) (fig. 2 in Tapponnier *et al.* 1990), ≈400 m below the 4092 m-high mountain summit. At
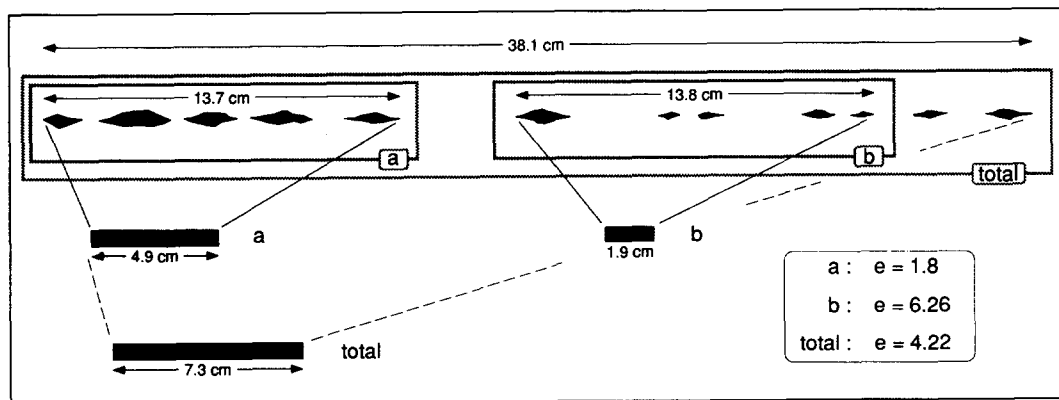

Fig. 5. Examples of errors due to sampling bias of irregularly spaced boudins of various sizes. Artificial sample has been drawn to enlarge possible errors. Sample segments a and b, respectively, under- and overestimate finite strain obtained with the longer trial segment (insert shows elongations obtained for segments a, b and total trail). Segments a and b, respectively, with high and low densities of boudin elements, are clearly too short to provide a good estimate of elongation.
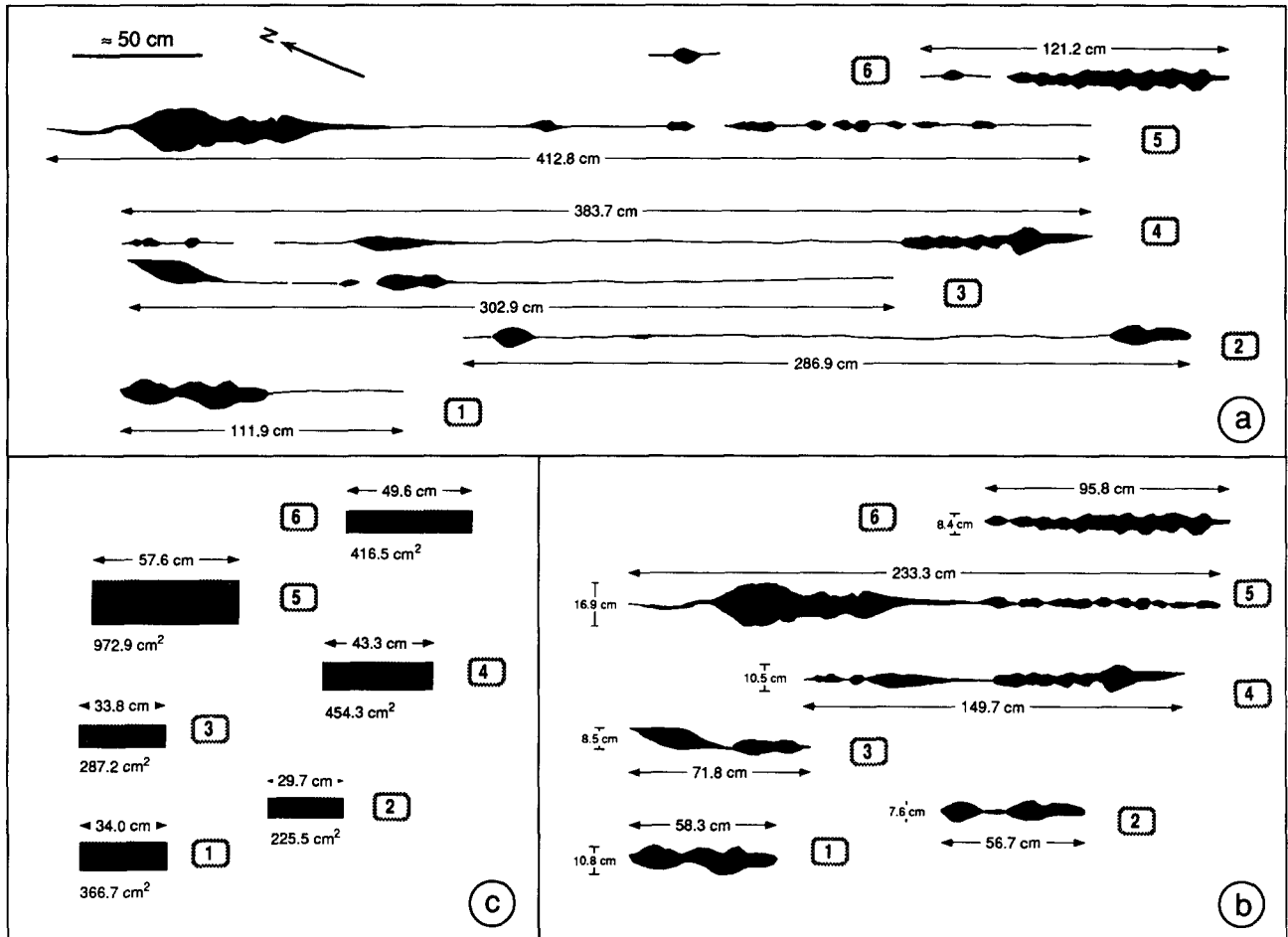
Fig. 6. Sets of amphibolite boudin trails (samples C1–C6, site 1, Ailao Shan). (a) Digitized boudin trails (derived from field mapping); (b) fit of boudin elements; (c) surface-balanced restoration. Note that samples C1 and C6, which comprise only one principal boudin element, yield underestimates of finite stretching.

this site, the only two boudin trails measured give extension values of 429 and 654%; the corresponding mean extension and quadratic extension are thus 542% and 42.5, respectively.

The leucocratic veins at sites 2 and 3 were emplaced during deformation as a result of partial melting. At site 2 for instance, several generations of veins are observed (Figs. 3, 7 and 8), ranging from strongly deformed (such as samples D and E1–E3) to gently deformed (e.g. samples E4 and E5) or even undeformed. The strongly deformed veins are syntectonic and record only the deformation increments post-dating their formation.

The amphibolite layers at site 1 (Figs. 4 and 6) are part of the compositional banding of the mylonitic para-

gneisses, which display metamorphic assemblages typical of amphibolite facies (Leloup & Kienast submitted). In the metapelitic layers (quartz–K-feldspar–plagioclase–biotite–garnet–sillimanite), biotite and sillimanite are clearly coeval with left-lateral shear (Leloup & Kienast submitted). Thus, the mylonitic banding, made of alternating metapelitic and amphibolite layers which parallel the foliation, probably formed by transposition of an original layering during the high-grade syntectonic metamorphism. Both the formation of this mylonitic banding, and its subsequent boudinage are due to the same progressive shear event. It follows that the amphibolite layers are likely syntectonic markers formed during the progressive deformation, as are the
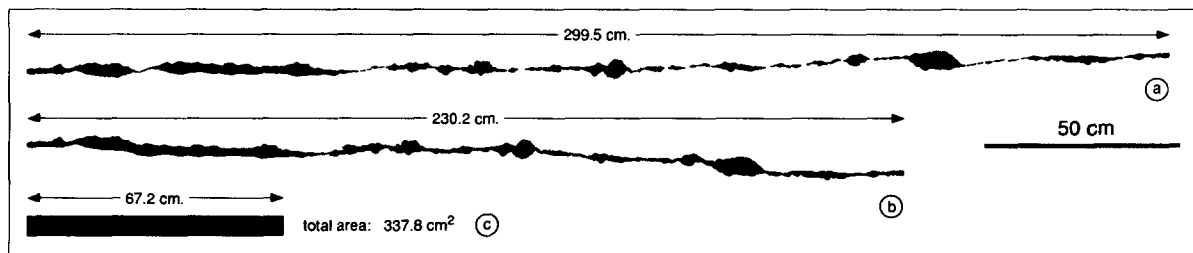

Fig. 7. Example of boudinaged leucocratic vein (sample D2, site 2, Ailao Shan). (a) Digitized boudin trail (drawn from a series of outcrop photographs, Fig. 3a); (b) fit of boudin elements; (c) surface-balanced restoration.
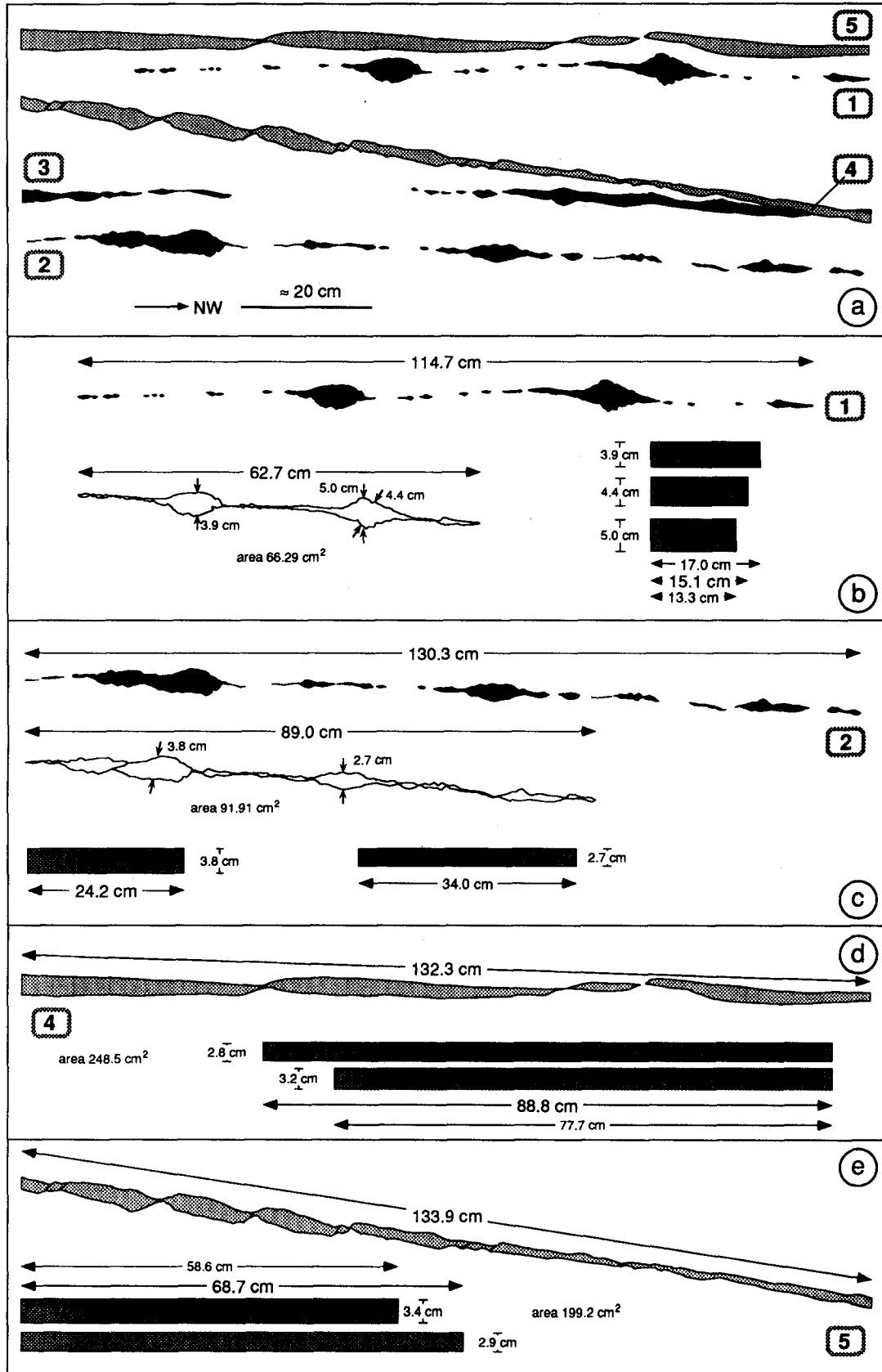
Fig. 8. (a) Set of stretched leucocratic veins (samples E, site 2, Ailao Shan), drawn from a series of outcrop photographs (Fig. 3b). Late syntectonic veins (samples E4 and E5, light shade) are clearly less elongated than others presumably emplaced earlier during progressive shear (E1–E3, dark shade). Such late veins show pinch and swell structures with back-rotation of the swells and shear planes located in the pinches (Hanmer 1986). See discussion in text (geological setting). (b) Restoration of boudin trail E1. Several possible restorations correspond to several possible initial thicknesses. (c) Restoration of boudin trail E2. (d) & (e) Restorations of late syntectonic veins (E4 and E5).
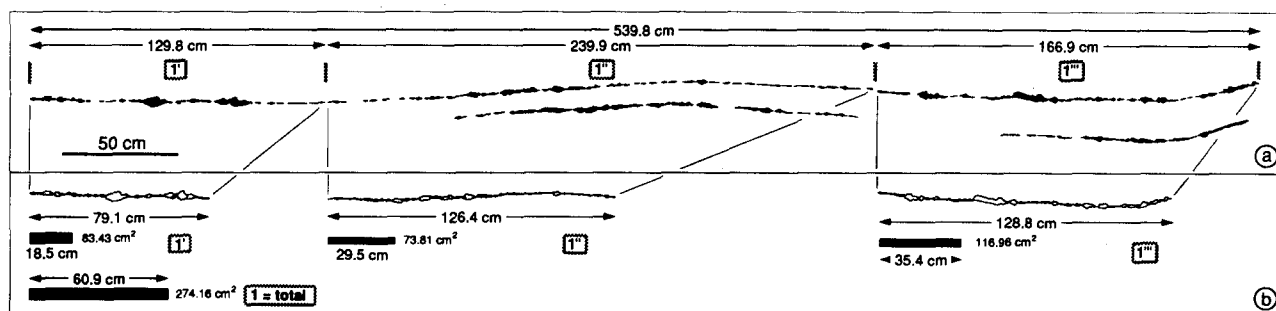
Fig. 9. Example of boudinaged leucocratic veins from the Wang Chao shear zone (Sample A). (a) Digitized boudin trails (drawn from a series of outcrop photographs); (b) restoration of trail A1. Note that restorations of parts of trails A1 (1', 1" and 1''') give smaller extension values than restoration of the whole trail (see text).

leucocratic veins. The boudinage of both should have recorded only part of the bulk finite strain.

It is not straightforward to compare results from the different sites, as these sites are up to a few hundred kilometres apart. Moreover, the stretched markers are different at site 1 (amphibolite layers) and at sites 2 and 3 (leucocratic veins). Clearly, the larger mean extension values at site 1 could be due either to locally more intense deformation, or to a longer strain history for the amphibolite layers that probably formed earlier than the leucocratic veins during the progressive deformation. In fact, it seems clear that the leucocratic veins at sites 2 and 3 were emplaced during a late stage of prograde metamorphism (Tapponnier et al. 1990, Leloup 1991, Leloup et al. submitted) and thus began to stretch later than the amphibolite layers did at site 1. Note also that both sites 2 and 3, although ≈300 km apart, yield comparable mean extension values for syntectonic leucocratic veins.

Wang Chao shear zone

Reliable extension values obtained for the Wang Chao shear zone (site 4, or Lancang site, Fig. 1c) range between 265 and 786% (Table 2 and Figs. 9, 10 and 11). These results yield a mean extension value of 430% for this site (mean quadratic extension: 30.9).

All the extension values at this site are derived from leucocratic veins. Since we observed outside the shear zone the same type of veins, although undeformed (Fig. 2a), and in view of the low grade of metamorphism,

it is likely that the stretched veins measured are pretectonic. Thus, the rather wide range of extension values cannot be related to the existence of several generations of syntectonic veins as in the Ailao Shan. Rather, instead it probably reflects strain heterogeneities at the outcrop scale (of the order of 20,000 m^2) or errors due to sampling bias and other uncertainties. In any case, this site being ≈2 km away from the central, ultramylonitic, part of the shear zone, the results probably underestimate the average strain in the Wang Chao shear zone.

BOUNDS ON FINITE SHEAR STRAIN IN THE AILAO SHAN AND WANG CHAO ZONES

The restoration of stretched layers using the surface-balancing method above yields large finite elongations, ranging from 250 to 870%. Therefore, it quantitatively documents the existence of large finite strains in the two shear zones we have studied. In most large-scale shear zones, the high state of strain in the rocks is usually inferred from qualitative observations such as the existence of mylonites, sheath folds, rolling structures or foliation boudinage. The fact that we could measure large finite strains in such a zone clearly supports this type of inference. Note that large layer-parallel elongations imply very large shear strain in the case of simple shear. Here, the layers are nearly parallel to the mylonitic foliation, which is itself close to the shear plane. This is thus reminiscent of the case studied by Gaudemer & Tapponnier (1987).
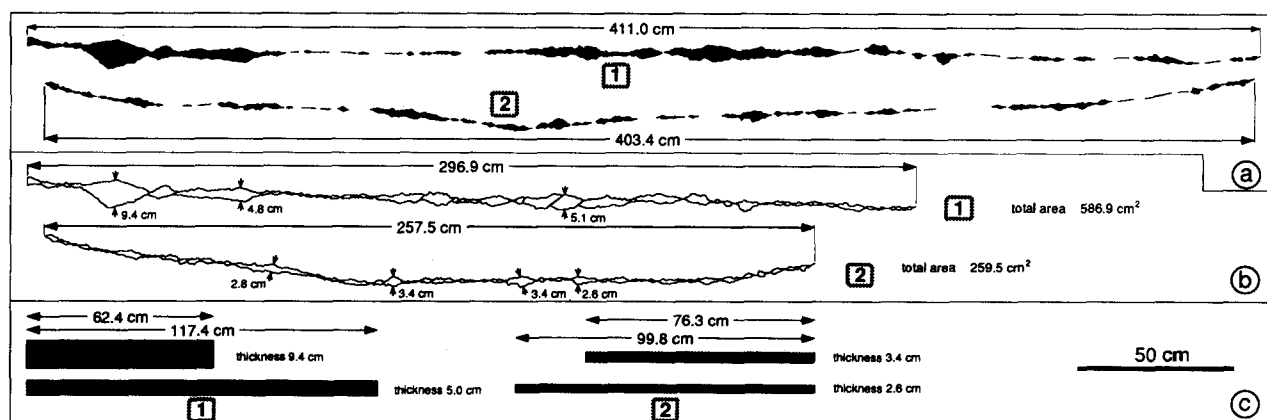

Fig. 10. Sample B, Wang Chao shear zone. (a) Digitized boudin trails (drawn from a series of outcrop photographs); (b) fit of boudin elements; (c) surface-balanced restoration.
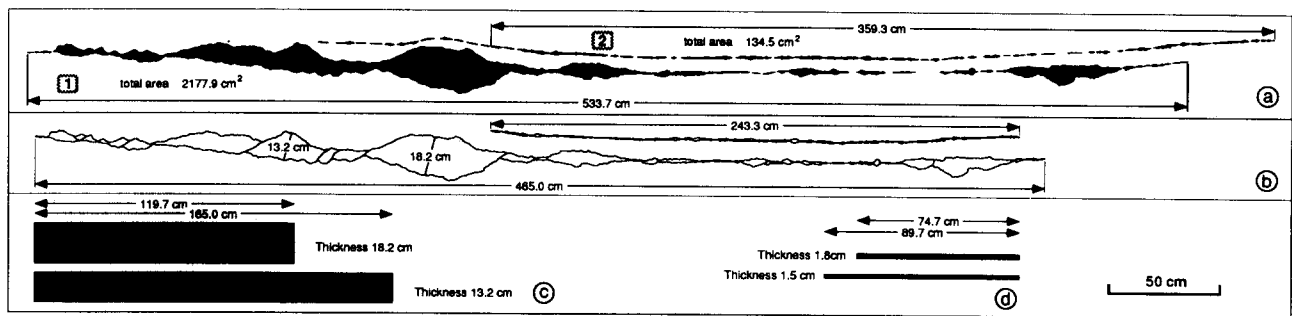
Fig. 11. Sample C, Wang Chao shear zone. (a) Digitized boudin trails (drawn from a series of outcrop photographs); (b) fit of boudin elements; (c) & (d) surface-balanced restoration.

To better constrain the kinematics of either zone, the next goal in our study is to place quantitative bounds on the shear strains compatible with the values of measured elongation. Solutions to this problem are non-unique because the finite elongation of a stretched marker depends on its initial orientation relative to the strain axes, and on the deformation regime (e.g. pure shear or simple shear, vorticity. . .) (e.g. Talbot 1970, Ramsay & Huber 1983, Passchier 1990). In the following discussion, we address the problem of the initial orientation of the markers. Although it might be argued that it is difficult to put definitive constraints on the deformation regime from outcrop observations only, the observations we made lead us to assume that the deformation regime in the Red River–Ailao Shan and Wang Chao shear zones was close to simple shear. That assumption receives particularly strong support from the great length of the two shear zones. Indeed, in most large-scale strike-slip shear zones, the geometric constraints at crustal or lithospheric scales (i.e. zones that are several hundreds of kilometres long with constant deformation characteristics, large offsets, no detectable lengthening of the shear zone walls and little crustal thickening, if any) are best accounted for by near-simple shearing.

Let us look firstly at the implications of the elongations we have measured if we assume that deformation occurred by plane simple shear. The layer parallel elongation (e) then depends only on the initial orientation of the markers and on the shear strain (γ).

The way to calculate the quadratic extension ($\lambda = (1 + e)^2$) of a line marking an angle α with the shear plane follows Ramsay & Huber (1983) and is presented in the Appendix.

From equation (A3) (Appendix), sets of curves $\lambda = f(\gamma)$ for different initial angles α may be derived (Fig. 12). Quadratic extensions measured in the Ailao Shan and Wang Chao shear zones are plotted on the diagrams of Figs. 12(a) & (b), respectively.

To estimate the simple shear strain (γ) corresponding to these values, let us now discuss step by step plausible values of initial angles between the stretched layers and the shear plane (Table 3).

(1) First note that we have never restored folded-then-boudinaged layers. In the case of simple shear, this implies that initial angles are always $\alpha \leq 90°$ (Talbot 1970, Passchier 1990). The most conservative minimum shear strain values (Table 3) are thus $\gamma = 8.3 \pm 1.4$ for

the amphibolite boudins at site 1; $\gamma = 5.5 \pm 1.8$ and $\gamma = 6.4 \pm 1.2$ for stretched syntectonic veins at sites 2 and 3; and $\gamma = 5.5 \pm 3$ for veins at the Wang Chao site. Note that, if some veins were initially located in the shortening sector and thus thickened before their boudinage, we have measured the strain increments accumulated after they moved into the extensional sector. The shear strain estimated for such veins and for $\alpha \leq 90°$ would thus reflect these later increments.

(2) According to Leloup (1991) and Leloup & Kienast (submitted), the latest, least deformed, leucocratic veins generally lie at a low angle to the mylonitic foliation in the Ailao Shan shear zone. If we consider that the stretched veins we measured were emplaced with the same geometry relative to the shear plane, and thus taking a maximum initial angle $\alpha = 45°$, we may deduce shear strains of $\gamma = 7 \pm 2.8$ and $\gamma = 8 \pm 1.7$, respectively, for the anatectic veins at site 2 (Ailao Shan) and site 3 (Diancang Shan) (Table 3). As these stretched veins were emplaced late during the deformation, these later values correspond only to late shear strains.

(3) The amphibolite layers at site 1 clearly formed during progressive deformation involving high-grade metamorphism and transposition of the initial layering of a series of volcanic and sedimentary rocks (Tapponnier et al. 1990, Leloup & Kienast submitted, Leloup et al. submitted). It is thus the combination of prograde metamorphism and shear strain that produced the mylonitic banding subsequently stretched by later increments of the same continuing shear. The boudinage of the amphibolite bands is thus comparable to foliation boudinage affecting rocks already foliated during the progressive deformation (Platt & Vissers 1980, Gaudemer & Tapponnier 1987, Lacassin 1988). This implies that the amphibolite bands lay parallel to the foliation at initial angles $\alpha < 45°$ before boudinage. A simple shear strain $\gamma \approx 11 \pm 2$ is thus deduced. In fact, it is likely that a minimum shear strain of $\gamma \approx 4$ was necessary to produce strong foliation, and to start transposition and the formation of compositional banding. Hence, a maximum initial angle $\alpha \approx 15°$, corresponding to the angle between the foliation and the shear plane for a simple shear of $\gamma \approx 4$, seems much more plausible for the layered amphibolites. Using this value for α, the shear strain corresponding to the stretched amphibolite boudins at site 1 in the Ailao Shan would be $\gamma = 28.8 \pm 6$ (Table 3). A finite simple shear strain $\gamma = 33 \pm 6$ is obtained by

adding to the boudinage strain the shear strain ($\gamma \approx 4$) necessary to form the foliation. Recall from the discussion of uncertainties earlier in this paper that even this value is likely to be a lower bound of the actual finite shear strain.

(4) Most of the leucocratic veins observed outside the Wang Chao shear zone are parallel to the foliation in the surrounding gneisses. The angle between this 'old' foliation and the shear zone is of the order of 45°. Using this value for the initial angle of the stretched veins, we may estimate a minimum shear strain $\gamma = 7 \pm 4$ in this zone.

Thus far, we have assumed that the observed finite strain in both shear zones was due to simple shear. Since the markers we studied were clearly formed during the progressive shearing, their finite elongation cannot be due to a complex strain history such as flattening followed by simple shear. A component of volume loss normal to the shear zone walls could only have led to underestimates of the initial thickness of the markers and thus their elongation. The calculation of layer-parallel quadratic extension for simple-shear with a component of volume loss normal to the shear zone is given in the Appendix (equation A7). Dilation (Δ) may vary between a maximum of -0.5 (50% of volume loss) and 0 (no volume loss). In equation (A7), $(1 + \Delta)^2$ is negligible compared to γ^2, and layer-parallel quadratic extensions are thus very close to those determined for isovolumetric simple shear, except for low values of λ
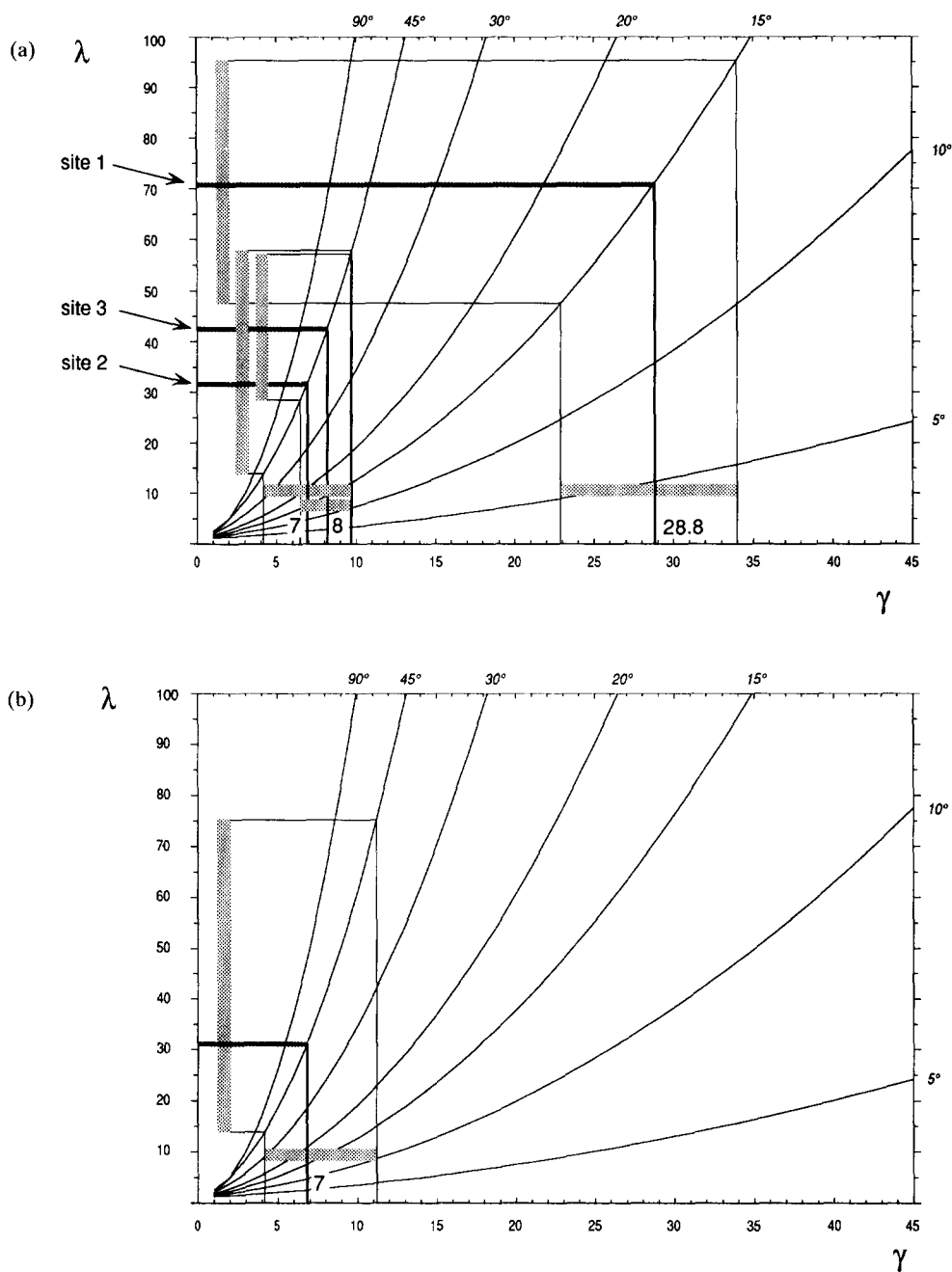

Fig. 12. Curves showing relationship between λ and γ for given initial angles (α, numbers in italic) between layer and simple shear plane. All boudinaged layers are taken to be initially located in the incremental extension sector ($\alpha \leq 90°$). (a) Plot of mean values of layer-parallel extensions measured at sites along the Red River–Ailao Shan shear zone. Shaded bars show range of results for each site. (b) Plot of mean value of layer-parallel extensions measured at the Lancang site in the Wang Chao shear zone. Symbols as in (a).

Table 3. Estimates of simple shear strain deduced from mean elongation values. Uncertainty results from range of
values obtained at each site

α (initial angle) (°)	Site 1 (amphibolites) Ailao Shan	Site 2 (syntectonic veins) Ailao Shan	Site 3 (syntectonic veins) Diancang Shan	Site 4 Wang Chao
90	$\gamma = 8.3 \pm 1.4$	$\gamma = 5.5 \pm 1.8$	$\gamma = 6.4 \pm 1.2$	$\gamma = 5.5 \pm 3$
45	$\gamma = 11 \pm 2$	$\gamma = 7 \pm 2.8$	$\gamma = 8 \pm 1.7$	$\gamma = 7 \pm 4$
15	$\gamma = 28.8 \pm 6$ + $\gamma \approx 4$ to form foliation $\gamma \approx 33 \pm 6$			

and γ. We have verified this approximation by calculating curves $\lambda = f(\gamma)$, which are almost identical to those of Fig. 12. It follows that such a volume loss would not change the minimum estimates of the shear strain.

Nevertheless, a deviation from a strict simple shear regime cannot be completely excluded. Such a deviation could have led us to overestimate the shear strain. We examine and illustrate in Fig. 13 and in the Appendix the effect of a component of flattening normal to the walls of the shear zone, superimposed on dominant simple shear. The shear strain value of $\gamma \approx 29$ estimated from the amphibolite boudins at site 1 (Ailao Shan) for strict simple shear is reduced by such flattening. It becomes ≈ 24 and ≈ 21 for increments of flattening of 5 and 10%, respectively, with each unit increment of shear (Fig. 13 and Appendix). Note that such flattening values would imply that the width of the shear zone was reduced by half, a large amount, after shear strains of 20 or 10, respectively. Concurrently, the length of the shear zone

walls would have doubled, and this lengthening would have been absorbed by penetrative deformation of regions located on both sides of the shear zone. As there is no evidence for such regional lengthening, we infer that a shear strain of 21, estimated for flattening increments of 10%, to be significantly less than the actual finite shear strain at site 1 in the Ailao Shan shear zone. A minimum shear strain of 25 is thus obtained by adding to this value the shear strain ($\gamma \approx 4$) necessary to form the foliation.

DISCUSSION: A FIRST-ORDER ESTIMATE OF MINIMUM TERTIARY LEFT-LATERAL DISPLACEMENT BETWEEN INDOCHINA AND SOUTH CHINA

From a qualitative point of view, most of the mylonitic paragneisses that form the core of the Ailao Shan and
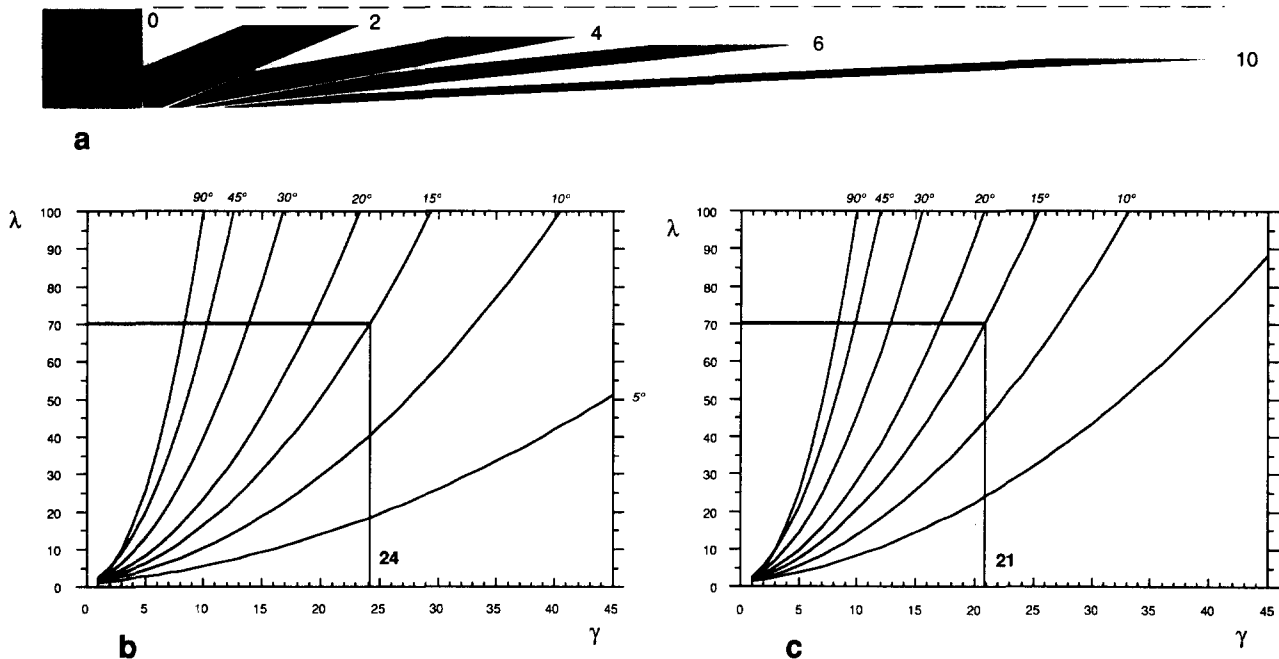

Fig. 13. Influence of component of flattening perpendicular to shear zone. (a) Plane rotational strain regime including flattening component perpendicular to shear plane (see the Appendix). Pure shear (flattening) increment here is 10% for each unit increment of shear (increments represented correspond to: $\gamma_r = 2$ and $e = 0.2$; $\gamma_r = 4$ and $e = 0.4$; $\gamma_r = 6$ and $e = 0.6$; $\gamma_r = 10$ and $e = 1$). (b) & (c) Curves $\lambda = f(\gamma_r)$ corresponding to strain regime of (a) and equations (A1) and (A5). As discussed in the Appendix, the rotational shear strain equivalent (γ_r) is graphically derived to allow comparison with estimates made with simple shear. (b) & (c) Correspond to pure shear increments of 5 and 10% for each unit increment of shear, respectively. Mean values of layer-parallel extensions measured at site 1 in the Ailao Shan shear zone are reported on both diagrams. Note that corresponding mean values of γ_r (about 24 and 21, respectively) are up to 25% less than in a strict simple shear regime.

Diancang Shan display states of strain comparable to those of the mylonites that contain the boudin trails we have studied. Moreover, the Red River–Ailao Shan shear zone also comprises localized ultramylonitic zones in which the finite strain is much larger. Thus, we infer the shear strain values obtained from boudinage to be acceptable first-order estimates of minimum average shear strain for the whole shear zone, which is 10 km wide. Assuming homogeneous simple shear the stretching of the amphibolites would imply a minimum left-lateral displacement of 330 ± 60 km between regions north and south of this zone. This minimum estimate would be reduced to 250 km if flattening perpendicular to the shear zone occurred in addition to shear within a general non-coaxial flow regime. Note that the order of magnitude of such lower bounds is consistent with estimates of the bulk displacement along the shear zone, that range between 500 and 740 km (Tapponnier et al. 1986, 1990, Peltzer & Tapponnier 1988, Leloup 1991). Ductile strain in the 10 km wide shear zone would thus have absorbed at least ≈30–60% of the bulk displacement. The shear strains deduced from the elongation of anatectic veins ($\gamma \approx 5.5$–8, Table 3) would imply that left-lateral displacement after the emplacement of these veins was of the order of 55–80 km. This late movement probably occurred after 23 Ma, given the ages obtained from these veins (Schärer et al. 1990).

If taken to represent the average shear strain in the ≈5 km wide Wang Chao shear zone, the shear strain ($\gamma = 7$) consistent with boudinage of the pretectonic veins would imply a minimum of ≈35 ± 20 km of left-lateral displacement. Such a displacement is small when compared to the offsets of geological markers (160–200 km; Tapponnier et al. 1986, Peltzer et al. 1988). That the measured value underestimates the average shear strain is no surprise, as the site studied was not situated in the most deformed ultramylonitic central part of the shear zone where measurements were not feasible.

Clearly, measurements at several other sites across several other sections of either shear zone are required to constrain more firmly the first order estimates of shear strain and displacement obtained in this study. It is also clear that our fundamental assumption of simple shear has to be corroborated by further work. Nevertheless, these estimates are compatible with the view that several hundreds and several tens of kilometres of left-lateral movement, respectively, occurred on the Red River–Ailao Shan shear zone and the Wang Chao shear zone. Radiometric dating of the crystallization of uranium-bearing minerals in the late anatectic veins (Schärer et al. 1990) implies that the bulk of the motion on the former zone occurred in the Oligo-Miocene (Tapponnier et al. 1990). Although the age of greenschist metamorphism along the Wang Chao zone is still pending, large Tertiary left-lateral movement along both zones would be consistent with the idea that, as India collided with the Asian continent, it rotated and pushed large slices of Indochina southeastwards out of its path, ultimately leading to the formation of the South China Sea (Briais 1989, Briais et al. in press). This is as predicted by

laboratory indentation experiments of Plasticine models (Tapponnier et al. 1982, 1986, Peltzer & Tapponnier 1988).

REFERENCES

Bell, T. H. & Etheridge, M. A. 1973, Microstructures of mylonites and their descriptive terminology. *Lithos* 6, 337–348.

Berthé, D., Choukroune, P. & Jegouzo, P. 1979. Orthogneiss, mylonite and non-coaxial deformation of granites: the example of the South Armorican Shear Zone. *J. Struct. Geol.* 1, 31–42.

Brias, A. 1989. Cinématique d'ouverture de la Mer de Chine du Sud (NanHai). Implications pour la tectonique tertiaire de l'Asie. Unpublished Doctorat de l'Université de Paris 6.

Briais, A., Patriat, P., Tapponnier, P. In press. Updated interpretation of magnetic anomalies and seafloor spreading stages in the South China Sea, implications for the Tertiary tectonics of SE Asia. *J. geophys. Res.*

Burg, J.-P. & Laurent, P. 1978. Strain analysis of a shear zone in a granodiorite. *Tectonophysics* 47, 15–42.

Cobbold, P. & Quinquis, H. 1980. Development of sheath folds in shear regimes. *J. Struct. Geol.* 2, 119–126.

Coward, M. P. 1976. Strain within ductile shear zones. *Tectonophysics* 34, 181–197.

Department of Mineral Resources. 1982. Geological Map of Thailand 1/1,000,000.

Escher, A. & Watterson, J. 1974. Stretching fabrics, folds and crustal shortening. *Tectonophysics* 39, 223–231.

Ferguson, C. C. 1981. A strain reversal method for estimating extension from fragmented rigid inclusions. *Tectonophysics* 79, T43–T52.

Fry, N. 1979. Random point distributions and strain measurements in rocks. *Tectonophysics* 60, 89–105.

Gaudemer, Y. & Tapponnier, P. 1987. Ductile and brittle deformations in the northern Snake Range, Nevada. *J. Struct. Geol.* 9, 159–180.

Hanmer, S. 1986. Asymmetrical pull-aparts and foliation fish as kinematic indicators. *J. Struct. Geol.* 8, 111–122.

Hanmer, S. 1990. Natural rotated inclusions in non-ideal shear. *Tectonophysics* 176, 245–255.

Hanmer, S. & Passchier, C. 1991. Shear-sense indicators: a review. *Geol. Surv. Pap. Can.* 90–17.

Harris, L. B. & Cobbold, P. R. 1984. Development of conjugate shear bands during bulk simple shearing. *J. Struct. Geol.* 7, 37–44.

Lacassin, R. 1988. Large-scale foliation boudinage in gneisses. *J. Struct. Geol.* 10, 643–647.

Lacassin, R., Leloup, P. H., Briais, A. & Tapponnier, P. 1991. Bounds on strike-slip displacements along large Tertiary shear zones in SE Asia. Abstract EUG VI. *Terra Abs.* 3, 258.

Lacassin, R. & Mattauer, M. 1985. Kilometre-scale sheath fold at Mattmark and implications for transport direction in the Alps. *Nature* 316, 739–742.

Lacassin, R. & Van Den Driessche, J. 1983. Finite strain determination of gneiss: application of Fry's method to porphyroid in the southern Massif Central (France). *J. Struct. Geol.* 5, 245–253.

Leloup, P. H. 1991. Cinématique des déformations 'Himalayennes' dans la zone de cisaillement crustale de l'Ailao Shan–Fleuve Rouge. Unpublished Doctorat de l'Université de Paris 6.

Malavieille, J. 1987. Extensional shearing deformation and kilometer-

scale 'a'-type folds in a Cordilleran metamorphic core complex (Raft River mountains, northwestern Utah). *Tectonics* **6**, 423–448.

Malavieille, J., Lacassin, R. & Mattauer, M. 1984. Signification tectonique des linéations d'allongement dans les Alpes occidentales. *Bull. Soc. géol. Fr.* **26**, 895–906.

Mattauer, M. 1975. Sur le mécanisme de formation de la schistosité dans l'Himalaya. *Earth Planet. Sci. Lett.* **28**, 144–154.

Mattauer, M., Faure, M. & Malavieille, J. 1981. Transverse lineation and large scale structures related to Alpine obduction in Corsica. *J. Struct. Geol.* **3**, 401–409.

Passchier, C. W. 1990. Reconstruction of deformation and flow parameters from deformed vein sets. *Tectonophysics* **180**, 185–199.

Passchier, C. W. & Simpson, C. 1986. Porphyroclast systems as kinematic indicators. *J. Struct. Geol.* **8**, 831–843.

Peltzer, G. & Tapponnier, P. 1988. Formation and evolution of strike-slip faults, rifts, and basins during the India–Asia collision: an experimental approach. *J. geophys. Res.* **93**, 15,085–15,117.

Platt, J. P. & Vissers, R. L. M. 1980. Extensional structures in anisotropic rocks. *J. Struct. Geol.* **2**, 397–410.

Riedel, W. 1929. Zur Mechanik geologischer Brucherscheinunger. *Zentbl. Miner. Geol. Paläont.* **1929B**, 354–368.

Quinquis, H., Audren, C., Brun, J. P. & Cobbold, P. 1978. Intensive progressive shear in Ile de Groix blueschists and compatibility with subduction or obduction. *Nature* **273**, 43–45.

Ramsay, J. G. 1967. *Folding and Fracturing of Rocks*. McGraw-Hill, New York.

Ramsay, J. G. & Allison, I. 1979. Structural analysis of shear zone in an alpinised hercynian granite. *Schweiz. miner. petrogr. Mitt.* **59**, 251–279.

Ramsay, J. G. & Huber, M. I. 1983. *The Techniques of Modern Structural Geology, Volume 1: Strain Analysis*. Academic Press, London.

Saltzer, S. D. & Hodges, K. V. 1988. The Middle Mountain shear zone, southern Idaho: Kinematic analysis of an early Tertiary high-temperature detachment. *Bull. geol. Soc. Am.* **100**, 96–103.

Schärer, U., Tapponnier, P., Lacassin, R., Leloup, P. H., Zhong, D. & Ji, S. 1990. Intraplate tectonics in Asia: a precise age for large-scale Miocene movement along the Ailao Shan-Red River fault zone, China. *Earth Planet. Sci. Lett.* **97**, 65–77.

Simpson, C. & Schmid, S. M. 1983. An evaluation of criteria to deduce sense of movement in sheared rocks. *Bull. geol. Soc. Am.* **94**, 1281–1288.

Talbot, C. J. 1970. The minimum strain ellipsoid using deformed quartz veins. *Tectonophysics* **9**, 47–76.

Tapponnier, P., Lacassin, R., Leloup, P. H., Schärer, U., Zhong, D. Wu, H., Liu, X., Ji, S., Zhang, L. & Zhong, J. 1990. The Ailao Shan-Red River metamorphic belt: Tertiary left lateral shear between Sundaland and South China. *Nature* **343**, 431–437.

Tapponnier, P., Peltzer, G. & Armijo, R. 1986. On the mechanics of the collision between India and Asia. In: *Collision Tectonics* (edited by Coward, M. P. & Ries, A. C.). *Spec. Publs geol. Soc. Lond.* **19**, 115–157.

Tapponnier, P., Peltzer, G., Le Dain, A. Y., Armijo, R. & Cobbold, P. 1982. Propagating extrusion tectonics in Asia: New insights from simple experiments with plasticine. *Geology* **10**, 611–616.

Tchalenko, J. S. 1970. Similarities between shear zones of different magnitudes. *Bull. geol. Soc. Am.* **81**, 1625–1640.

Van Den Driessche, J. 1986. Structures d'enroulement et sens de cisaillement. *C. r. Acad. Sci., Paris* **303**, 413–418.

Van Den Driessche, J. & Brun, J.-P. 1987. Rolling structures at large strain. *J. Struct. Geol.* **9**, 691–704.

White, S. H., Burrows, S. E., Carreras, J., Shaw, N. D. & Humphreys, F. J. 1980. On mylonites in ductile shear zones. *J. Struct. Geol.* **2**, 175–187.

Yan, Q., Zhang, G., Kan, R. & Hu, H. 1985. The crust structure of Simao to Malong profile, Yunnan province, China. *J. seism. Res.* **8**, 249–264.

Zhong Dalai, Tapponnier, P., Wu Haiwei, Zhang Liansheng, Ji Shaocheng, Zhong Jiayou, Liu Xiaohan, Schärer, U., Lacassin, R. & Leloup, P. 1990. Large-scale strike slip fault: the major structure of intracontinental deformation after collision. *Chinese Sci. Bull.* **35**, 304–309.

APPENDIX
TWO-DIMENSIONAL CALCULATION OF THE EXTENSION OF A LINE MAKING AN ANGLE α WITH THE SHEAR PLANE

(1) According to Ramsay & Huber (1983, p. 285, equation B11), the quadratic extension $(\lambda=(1+e)^2)$ of a line making an angle α with the x axis is given by:

$$\lambda = \tfrac{1}{2}(a^2 - b^2 + c^2 - d^2)\cos 2\alpha$$

$$+(ab + cd)\sin 2\alpha + \tfrac{1}{2}(a^2 + b^2 + c^2 + d^2), \quad (A1)$$

where $\quad \begin{vmatrix} a & b \\ c & d \end{vmatrix} \quad$ is the plane strain matrix. $\quad$ (A2)

(2) For simple shear (γ) parallel to x, equation (A1) becomes:

$$\lambda = -\tfrac{1}{2}\gamma^2\cos 2\alpha + \gamma \sin 2\alpha + \tfrac{1}{2}\gamma^2 + 1 \quad (A3)$$

$\begin{vmatrix} 1 & \gamma \\ 0 & 1 \end{vmatrix} \quad$ being the simple shear matrix. $\quad$ (A4)

(3) For plane rotational strain parallel to x that deviates from simple shear (Figs. 13 and A1), co-ordinate transformation equations may be derived graphically using the Ramsay & Huber technique (Ramsay & Huber, 1983, p. 283).

γ_r is a graphically determined rotational shear strain that allows comparison with simple shear strain and displacements in the deformed state. e is the component of extension parallel to the shear plane.

The co-ordinate transformation equations thus become:

$$x' = ax + by = (1 + e)x + \gamma_r y$$

$$y' = cx + dy = dy = (1 + e)^{-1}y \quad \text{(if no area change} \quad d = 1/a)$$

thus $\quad \begin{vmatrix} 1 + e & \gamma_r \\ 0 & (1 + e)^{-1} \end{vmatrix} \quad$ is the plane strain matrix. $\quad$ (A5)

The strain matrix may be used in equation (A1) to calculate quadratic extensions.

(4) For simple shear with a volume change component normal to the walls of the shear zone, according to Ramsay (1980), the strain matrix becomes:

$$\begin{vmatrix} 1 & \gamma \\ 0 & 1 + \Delta \end{vmatrix}, \quad (A6)$$

where Δ is the dilation component (less than 0 for volume loss)

As in the case of rotational strain, this strain matrix may be used in equation (A1) to calculate quadratic extensions. Equation (A1) thus becomes:

$$\lambda = \tfrac{1}{2}(1-\gamma^2 - (1 + \Delta)^2)\cos 2\alpha + \gamma \sin 2\alpha + \tfrac{1}{2}(1 + \gamma^2 + (1 + \Delta)^2). \quad (A7)$$
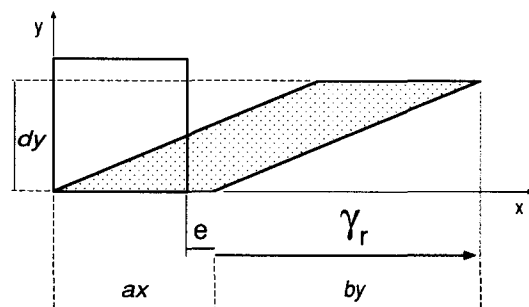

Fig. A1. Method used to determine the co-ordinate transformation equations and strain matrix for plane rotational strain. $a, b, c = 0$ and d are the four terms of the strain matrix (Ramsay & Huber 1983, p. 283).